PAPER

Check for updates

Anomalous kinetic roughening in growth of MoS₂ films under pulsed laser deposition†

Gobinda Pradhan,‡ Partha P. Dey [ID] ‡ and Ashwini K. Sharma [ID] *

Growth dynamics of thin films expressed by scaling theory is a useful tool to quantify the statistical properties of the surface morphology of the thin films. To date, the growth mechanism for 2D van der Waals materials has been rarely investigated. In this work, an experimental investigation was carried out to identify the scaling behavior as well as the growth mechanism of 2D MoS₂ thin films, grown on glass substrates by pulsed laser deposition for different deposition time durations, using atomic force microscopy images. The growth of MoS₂ films evolved from layer–by–layer to layer plus island with the increase in deposition time from 20 s to 15 min. The film surface exhibited anisotropic growth dynamics in the vertical and lateral directions where RMS roughness varied with deposition time as $w \sim t^{\beta}$ with the growth exponent $\beta = 0.85 \pm 0.11$, while the lateral correlation length ξ was $\xi = t^{1/z}$ with $1/z = 0.49 \pm 0.09$. The films showed a local roughness exponent $\alpha_{\text{loc}} = 0.89 \pm 0.01$, global roughness exponent $\alpha = 1.72 \pm 0.14$ and spectral roughness exponent $\alpha_s = 0.85 \pm 0.03$, suggesting that the growth of MoS₂ thin films followed intrinsic anomalous scaling behavior ($\alpha_s < 1$, $\alpha_{\text{loc}} = \alpha_s \neq \alpha$). Shadowing owing to conical incoming particle flux distribution towards the substrate during deposition has been attributed to the anomalous growth mode. The optical properties of the films, extracted from ellipsometric analysis, were also correlated with RMS roughness and cluster size variation which unveiled the important role played by surface roughness and film density.

1. Introduction

Transition metal dichalcogenides (TMDCs) are an emerging class of two-dimensional (2D) material with interesting electronic and optical properties.[1–3] Among all the TMDC materials, MoS₂ has drawn remarkable attention with its excellent semiconductor behavior like a tunable band gap of 1.2 (indirect)–1.9 (direct) eV, high electron mobility, high electronic on-off switching ratio, photoresponse *etc.*[4–6] These properties make it more suitable than graphene for logic device applications. The true 2D nature makes MoS₂ outperform Si transistors in terms of the nanoscale device limit.[7,8] Recently, many MoS₂-based devices have been demonstrated, including field effect transistors, integrated circuits and photo transistors.[9–13] MoS₂ nanosheets also have an established efficacy as a catalyst for hydrogen evolution reaction and an electrode in super-capacitors.[14–16] In the last few years, mono- and multilayered as well as bulk-like MoS₂ films deposited *via* pulsed laser deposition (PLD) and their advanced applications in modern electronics and the optoelectronics field have been reported.[17,18] The

Department of Physics, Indian Institute of Technology Guwahati, Guwahati – 781039, Assam, India. E-mail: aksharma@iitg.ac.in; Fax: +91-361-258-2749; Tel: +91-361-258-2724

‡ Equal contribution.

morphology and nanostructure of thin films strongly depend on the deposition method and growth conditions (*i.e.* duration, rate, temperature *etc.*).[19,20] The surface morphology of thin films can control many of the physical and chemical properties (such as optical, catalytic, mechanical, electronic, *etc.*) which can strongly affect the device performance of the respective films. Therefore, understanding the growth dynamics of the deposited thin films is very important.

The growth dynamics of thin films expressed by scaling theory is a useful tool to quantify the statistical properties of the surface morphology of thin films and to formulate theoretical models of growth modes for different inorganic materials such as metals, semiconductors, perovskite material *etc.*[21–25] Scaling is often described in terms of a scaling function, describing certain aspects of a rough surface, which generally evolves with time but remain invariant with time only under certain scale transformations. In the past few decades, several theoretical models were proposed to relate the thin film growth mechanism to a set of scaling exponents.[24,26–28] To the best of our knowledge, the growth mechanism of 2D van der Waals materials remains poorly investigated till date. The growth dynamics of MoS₂ films using scaling functions under PLD were never reported which motivated us to undertake the following study.

We report on the evolution of surface morphology of a bi-layer to bulk-like MoS₂ films to understand the growth dynamics and scaling behavior involved in MoS₂ thin film

growth under PLD. We have fitted the height–height correlation function (HHCF) with appropriate theoretical model to extract the interface width (w), lateral correlation length (ξ) as they evolve with deposition time. The film properties were quantified statistically in terms of short range (local) as well as long-range (global) roughness exponents (α_{loc} and α), growth exponent (β), dynamic scaling exponent (z), *etc.* to determine the type of scaling and growth mechanism involved. This understanding can enable one to attain controlled growth of a film required in different applications. Spectroscopic ellipsometry (SE) studies enabled us to estimate the refractive index (n) and extinction coefficient (k) spectra for various film thicknesses. Their variation with increasing film thickness is correlated with RMS roughness (interface width w) and island size (correlation length ξ) variation which unveiled the important role played by surface roughness and film density. Such correlations have been rarely reported for 2D material. Moreover, the SE studies are also used to support the anomalous scaling behavior of film growth as concluded from AFM analysis.

2. Experiment

MoS$_2$ thin films were deposited onto Corning glass substrate *via* PLD by focusing a 3rd harmonic of a Q-switched Nd:YAG laser (Spectra-Physics, pulse duration – 8 ns and repetition rate – 10 Hz) on polycrystalline MoS$_2$ target (pellet), at a laser fluence $\sim$ 2.2 J cm^{-2} under vacuum ($\sim 5 \times 10^{-6}$ mbar). The films were deposited for various deposition times of 20 s, 1, 2, 5, 10 and 15 min duration at a substrate temperature of 600 °C. Raman spectra of the films were recorded (Horiba Jobin Yvon, LabRam HR 800) in the backscattering geometry using an excitation wavelength of 488 nm. X-ray diffraction measurements were carried out with the Cu K$_\alpha$ line in an X-ray diffractometer (Rigaku TTRAX III) at a glancing incidence angle of $\omega = 1°$. The scanning range was 10° to 70° with an angular step of 0.03°. The surface morphology of all the films was recorded *via* AFM (Bruker-Innova) to study the dynamic scaling and growth mechanism of MoS$_2$ films deposited *via* PLD technique. The SE measurements were carried out over the spectral range of 1.32–3.50 eV using Variable Angle Spectroscopic Ellipsometer (Semilab SOPRA: GES-5E) equipped with goniometer at incident angles of 65°, 70°, and 75°. Data acquisition and analysis were performed using spectroscopy ellipsometry analyzer (SEA) software. The analysis of SE data was carried out by screening several realistic physical models for semiconductors to obtain the best fit.[29–32] In the present case, only the SE spectra recorded at incident angles of 70° is presented though the corresponding spectra at incident angles of 65°and 75° were also fitted with the same modeling which exhibited similar results.

3. Results and discussions

3.1. Structural characterization of MoS$_2$ films

Fig. 1 shows Raman spectra of MoS$_2$ films for deposition time of 20 s, 1, 2, 5 min and MoS$_2$ pellet in backscattering configuration. Each spectra exhibit twin peaks corresponding to A$_{1g}$ and E$^1_{2g}$ Raman modes of MoS$_2$. The E$^1_{2g}$ and A$_{1g}$ Raman modes show
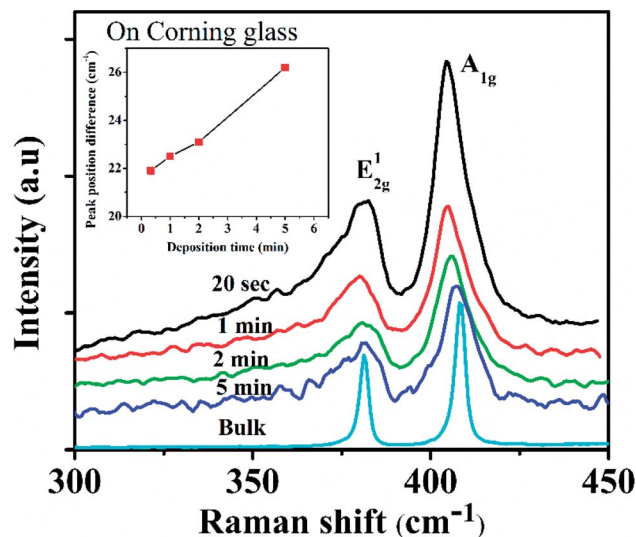

Fig. 1 Raman spectra of the MoS$_2$ films as a function of deposition time (t).

layer sensitive peak positions. The peak position difference of A$_{1g}$ and E$^1_{2g}$ of MoS$_2$ films increases with increase in layer numbers from monolayer to higher order.[33] The Raman peak position difference of the deposited films are shown in the inset of Fig. 1.

The peak positions corresponding to A$_{1g}$ mode were observed at 404.9, 405.4, 405.6 and 406.2 cm^{-1} while that corresponding to E$^1_{2g}$ at around 383, 382.9, 382.5 and 380 cm^{-1} for the films deposited for time duration of 20 s, 1, 2 and 5 minutes, respectively. The peak difference between the two Raman modes, ΔF, in the respective films were found to be 21.9, 22.5, 23.1 and 26.2 cm^{-1}, corresponding to bilayer, trilayer, multilayer and bulk-like MoS$_2$ films.[34,35] The Raman analysis of the films confirmed an increase in film thickness with the deposition time. Using surface profilometer the thicknesses of the films deposited for 1, 2, 5, 10 and 15 min deposition time are estimated to be 2.5, 6.4, 19.9, 39.6 and 81.2 nm, respectively while thickness of film deposited at 20 s could not be measured accurately due to much lower thickness (<2 nm). The XRD spectra of MoS$_2$ films (ESI Fig. S1†) exhibits peaks at $2\theta = 13.71°$ and 40.62° which corresponds to MoS$_2$ (002) and MoS$_2$ (103) planes, respectively, with former being more intense. The peak intensity of both peaks increased while the corresponding FWHM decreased with increasing deposition time as the MoS$_2$ film thickness increased exhibiting increase in crystallinity.

3.2. Scaling studies of MoS$_2$ film growth using AFM image analysis

The post growth surface morphology of the films was characterized systematically using AFM to study the surface microstructure and dynamics of the growth. Fig. 2(a)–(f) shows the AFM images of MoS$_2$ films grown onto the Corning glass surfaces at 600 °C substrate temperature with 20 s, 1, 2, 5, 10 and 15 min deposition times, respectively.

The AFM micrograph confirms that the grains are uniformly distributed within the film scanning area (2 μm × 2 μm). The
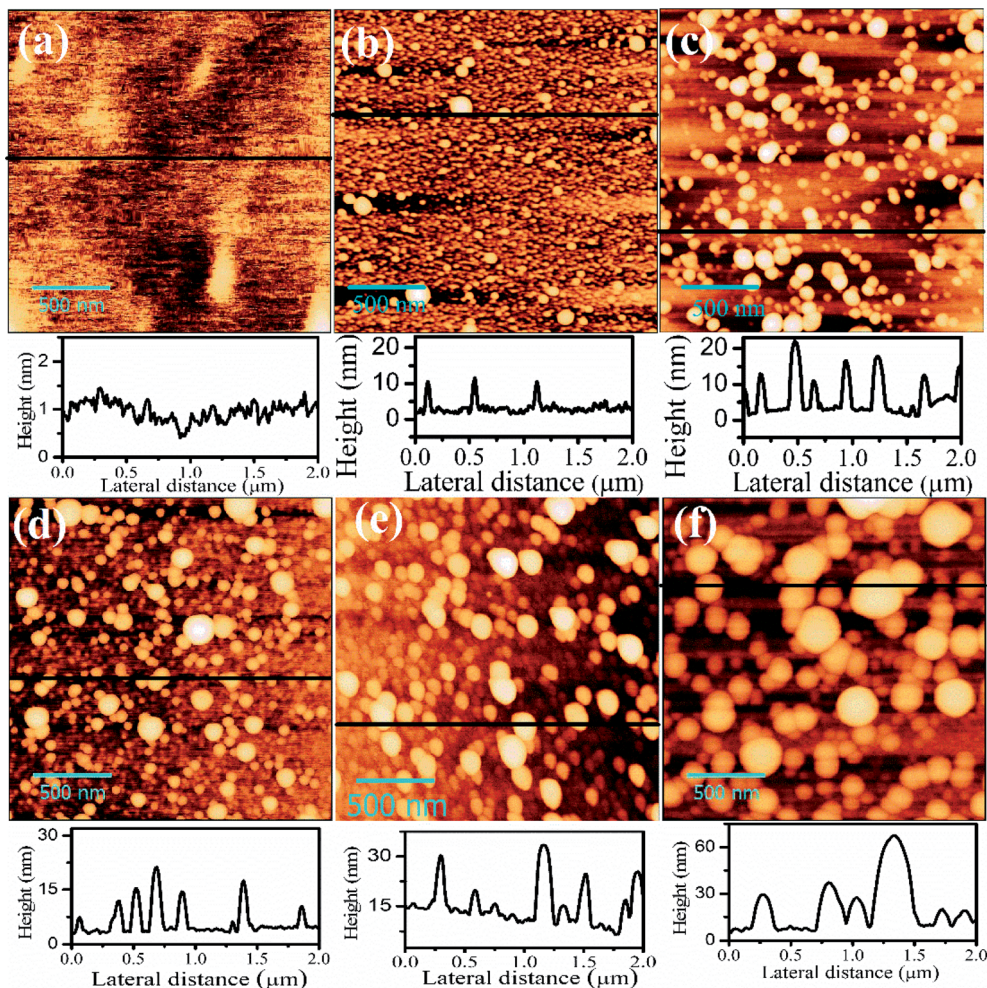
Fig. 2 AFM images of top surface of PLD MoS$_2$ films, showing the surface morphology for different deposition times (a) 20 s, (b) 1, (c) 2, (d) 5, (e) 10 and (f) 15 min. Each image consists of 2 × 2 μm scanned area and scale bar is 500 nm. Height profile of each image is shown at the bottom of the respective images.

scaling exponents (α_{loc}, β, $1/z$) have been estimated from the height–height correlation function (HHCF), $H(r,t)$ by analyzing the surface morphology recorded using AFM to understand the growth processes and the dynamic scaling behavior involved during PLD of MoS$_2$ films. $H(r,t)$ is defined as statistical average of the mean square of height difference between two positions (x, y) and (x', y') on the surface separated by a distance $r(= \sqrt{(x - x')^2 + (y - y')^2})$ along horizontal direction as $H(r,t) = \langle |h(r + r',t) - h(r',t)|^2 \rangle$, where $h(r + r',t)$ and $h(r',t)$ are the heights of the surface at (x, y) and (x', y') and each pair of points are obtained from AFM image. HHCF can be evaluated from AFM images by spatial averaging over one or several regions, which should be much larger than r to avoid edge effects. HHCF shows two distinct behaviors based on the relative magnitudes of r and the lateral correlation length ξ; (i) for $r \ll \xi$, $H(r,t) \sim [m(t)r]^{2\alpha}$; where $m(t)$ is the local slope and α_{loc} ($0 \le \alpha_{\text{loc}} \le 1$) is the local roughness exponent, which describes short-range roughness of a self-affine surface, and (ii) for $r \gg \xi$, $H(r,t) \sim 2w^2$, where $w = \sqrt{\langle [h(r,t)]^2 \rangle}$ is the RMS roughness (interface

width). w evolves following a simple dynamic scaling known as Family–Vicsek relation, $w = t^\beta f\left(\dfrac{r}{t^{\beta/\alpha_{\text{loc}}}}\right)$ where

$$f\left(\frac{r}{t^{\beta/\alpha_{\text{loc}}}}\right) \sim \begin{cases} \text{constant} & \text{when, } r \gg t^{\beta/\alpha_{\text{loc}}} \\ \left(\dfrac{r}{t^{\beta/\alpha_{\text{loc}}}}\right)^{\alpha_{\text{loc}}} & r \ll t^{\beta/\alpha_{\text{loc}}} \end{cases}$$

and $r \le L$ (L is system size) while α_{loc} and β are the roughness and growth exponents, respectively.[36,37] The above relation suggests that for small r (i.e. $r \ll t^{\beta/\alpha_{\text{loc}}}$), w is independent of deposition time t and scales as $r^{\alpha_{\text{loc}}}$, but for large r, β is independent of r and follow the power laws as $w \sim t^\beta$. The crossover between these two behaviors occurs at $r = \xi$, the lateral correlation length within which surface heights are significantly correlated. For dynamic scaling, the parameters w and ξ are dependent on the deposition time, t, and follow the power laws as $w \sim t^\beta$ and $\xi \sim t^{1/z}$.[37] The set of exponents α_{loc}, β and $1/z$, corresponds to a specific universality class and is suggestive of the underlying mechanism that governs the evolution of surface. The HHCF can be defined by exponential correlation model, which satisfies the requirement for self-affine surface and manifests anisotropic scale invariance, given by,[37]

$$H(r) = 2w^2 \left[1 - \exp\left[-\left(\frac{r}{\xi}\right)^{2\alpha} \right] \right] \tag{1}$$

From Fig. 3(a), it is observed that HHCF, $H(r,t)$ increases linearly with r at small r and saturates at large r, with the asymptotic behavior predicted by eqn (1).[37] It is clear from Fig. 3(a) that $H(r,t)$ shifts upward as film thickness increases with increasing growth time, which confirms that the RMS roughness increases as the films grow, indicating roughening in the growth process.

The HHCF curves were fitted using eqn (1), and $w(t)$, $\xi(t)$ as well as α_{loc} were estimated. The variation of these parameters with deposition time were studied to understand the growth dynamics. Fig. 3(b) exhibits variation of α_{loc} with time (t), while Fig. 3(c) and (d) shows log–log variations of w, and ξ versus t, respectively. From Fig. 3(b) it is observed that the value of α_{loc} for the film deposited for 20 s was 0.41 and beyond that, it rises sharply and remains almost similar for all deposition time at around ~0.89 ± 0.01. α_{loc} lies between 0 to 1, where, a smaller value of α_{loc} corresponds to the more locally rough surface while the larger α_{loc} of the present films corresponds to locally smooth surface. Fig. 3(c) shows the increasing nature of w from 0.27 to 18.6 nm as the film grows with t from 20 s to 15 min and it clearly indicates the film roughening during growth. The parameters w showed power law dependency as $w \sim t^\beta$ with $\beta = 0.85 \pm 0.11$. β is called growth exponent signifying the pace of surface roughening where $\beta > 0.5$ represents rapid roughening in thin films due to different non local effects like shadowing, high stickiness of substrate, bulk diffusion of incoming particles etc. Fig. 3(d) exhibits ξ versus t plot in logarithmic scale. Initially, at 20 s the value of ξ was 120.3 nm beyond which the value of ξ drops to 33.2 nm at 1 min deposition time. However, with increasing t from 1 to 15 min an increasing nature of ξ was observed, as shown in Fig. 3(d). This indicates that the lateral growth of the islands changes with time as $\xi \sim t^{1/z}$ where $1/z = 0.49 \pm 0.09$. $1/z$ is called dynamics scaling exponent which

corresponds to rate of lateral growth of correlated structure (islands). This confirms that as the deposition time increases, the islands grow both vertically as well as laterally and the overall film becomes rough. The lateral growth could be attributed to the increased nucleation of more incoming flux and the increase in crystallite size with increasing deposition time. The unusual large value of ξ at early stage of film growth at 20 s deposition time is due to layered (bilayer) MoS_2 film growth supported by Raman results (Fig. 1). At this nucleation and growth stage only lateral growth takes place (following Frank–Van Der Merwe model) while with an increase in deposition time the vertical growth of the MoS_2 film dominate over the lateral growth (following Sranski–Krastanov model) and the RMS roughness increases drastically as shown in Fig. 3(c).[38]

The TEM and FESEM images of films fabricated for 20 s (as shown in Fig. 4(a) and (b)) exhibit formation of bilayer without any cluster formation while that of 5 min film (Fig. 4(c) and (d)) show MoS_2 clusters of various sizes sparsely distributed in uniform layered background film. The magnified TEM image (Fig. 4(e)) also shows the multilayer formation beneath the clusters. Hence, the transition of growth mode from layer-by-layer in the film fabricated at 20 s to layer plus island type for that deposited for longer duration observed in TEM and FESEM images is complementing the AFM results.

For dynamic scaling to prevail, $\alpha_{loc} = \beta z$ but in our case $\alpha_{loc} \neq \beta z$, hence the dynamic scaling fails which implies that the scaling does not follow Family–Vicsek relation. In such a case, the height profile may follow another scaling hypothesis called anomalous scaling where the global and local interface widths scale differently and the global (α, β) and local $(\alpha_{loc}, \beta_{loc})$ exponents are also different from each other. Such behavior has been observed where the conventional scaling laws can be modified by introducing new behavior in the interface width, w, which is represented by the anomalous scaling ansatz:

$$w(r, t) = \begin{cases} t^{\beta*} r^{\alpha_{loc}}, & \text{if } r \ll \xi \ll L, \\ t^\beta, & \text{if } r \gg \xi \end{cases} \tag{2}$$
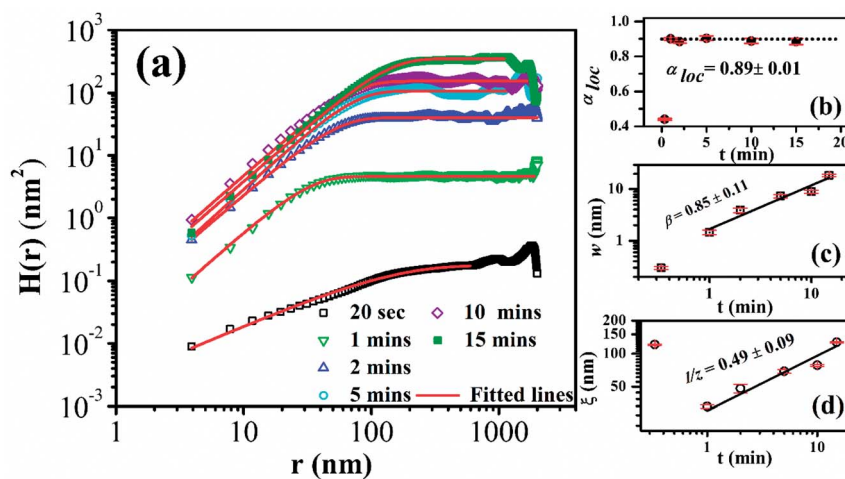

Fig. 3 (a) log–log plot of HHCF, $H(r)$ as a function of distance r with best fitted theoretical curve for MoS_2 thin films on Corning glass substrate with different deposition times (20 s to 15 min). The symbols are experimental data and the red solid lines are fitted with eqn (1). Plot of (b) roughness exponent α_{loc}, (c) surface roughness w, and (d) correlation length ξ as a function of deposition time, t.
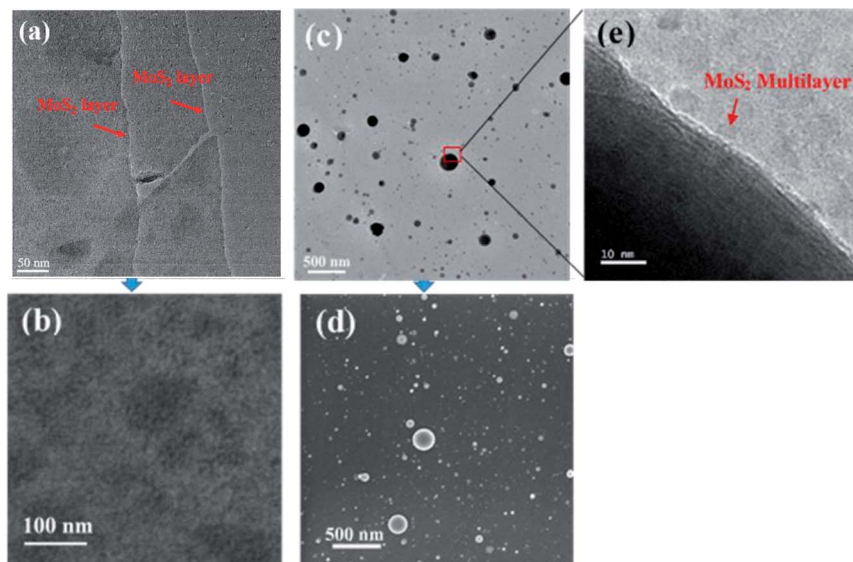
Fig. 4 (a) TEM and (b) FESEM image of MoS_2 film deposited for 20 s while (c) TEM and (d) FETEM image of MoS_2 film deposited for 5 min and (e) high magnified TEM image of MoS_2 cluster formed over the MoS_2 film deposited for 5 min.

where α_{loc} is the local roughness exponent and β^* is the anomalous growth exponent indicating the time dependence of the w at length scales smaller than ξ and is given by $\beta^* = \beta - \beta_{loc} = (\alpha - \alpha_{loc})/z = \beta - \alpha_{loc}/z$.[36,39–42] For such case, there exists a global roughness exponent $\alpha(\sim\beta z)$ different from local roughness exponent α_{loc}. Now, as we can see for Family–Vicsek case, $\beta^* = 0$, $\alpha = \alpha_{loc}$ and eqn (2) gives back $w(r,t)$ for dynamic scaling. The non-zero value of β^* ($\sim 0.41 \pm 0.02$) obtained from parameters estimated from HHCF suggest that the growth process follows anomalous scaling behavior which can be further categorized into super-rough, intrinsic anomalous or new class scaling as will be discussed later. In order to identify the growth mode, local slope $m(t)$ as a function of deposition time was plotted, as shown in ESI Fig. S2.† For exponential model expressing self-affine surface represented by eqn (1),

$$m = \frac{(w\sqrt{2})^{1/\alpha_{loc}}}{\xi}.$$[37] If $m(t)$ is independent of deposition time, it

is called stationary type of growth. In stationary growth, for $r < \xi$ the HHCF will merge for different t values. However, for the non-stationary case, $H(r)$ will shift upward as the local slope, $m(t)$, will change with the duration of deposition.[21] In the present case, the growth is obviously non-stationary as $m(t)$ was not constant. It was observed that the local slope, $m(t)$ increases with time and varies as, $m \sim t^{0.41\pm0.11}$ as depicted in ESI Fig. S2.† Such a behavior where local slope m evolves with a power law in time, $m(t) \sim t^{\beta^*}$ is observed for anomalous scaling.[37,39] From this observation β^* is found to be $\sim 0.41 \pm 0.11$ which is close to the value obtained from growth exponents.

Now if we consider the combination of growth exponents α, β and z where $\alpha = \beta z$, then under anomalous scaling also $w \sim t^\beta = t^{\alpha/z}$. As $\xi \sim t^{1/z}$, one can easily observe that $w \sim \xi^\alpha$ and the value of α can be found using the slope of $\log w$ versus $\log \xi$ as shown in Fig. 5. From the plot, the value $\alpha = 1.72 \pm 0.14$ was estimated, which is close with that obtained from $\alpha = \beta z \sim 1.70 \pm 0.13$. The

observed $\alpha > 1$ suggest domination of vertical growth over the lateral growth *i.e.* the films roughening increases with the deposition time in the MoS_2 films. The nonzero value of β^* (as a result of inequality of α and α_{loc}) indicates that scaling behaves anomalously and reconfirms the presence of a roughness exponent in global scale.

To further investigate the anomalous scaling behavior, the power spectral density function (PSDF) of the MoS_2 films of various thicknesses were plotted in reciprocal space, k. The power spectral density function (PSDF) given as[37] $P(k,t) = \frac{1}{(2\pi)^d}|\langle h(r,t)e^{-ikr}\rangle|^2$ (ref. 37) is related to d-dimensional Fourier transform of surface heights, $h(r,t)$ defined in reciprocal space, k. For an anomalous $(d + 1)$ dimensional system, the PSD for anomalous scaling can be represented in frequency and time scale as,[36,43,44]

$$\text{PSD}(k,t) \sim \begin{cases} t^{(2\alpha+d)/z} & kt^{1/z} \ll 1 \\ k^{-\gamma}t^{2\beta^*} & kt^{1/z} \gg 1 \end{cases} \quad (3)$$

where γ is $2\alpha_s + d$, d is spatial dimension for the scanned system, α_s is the spectral roughness exponent and $\beta^* = (\alpha - \alpha_s)/z$. On the basis of α_s, α_{loc} and α value the growth scaling
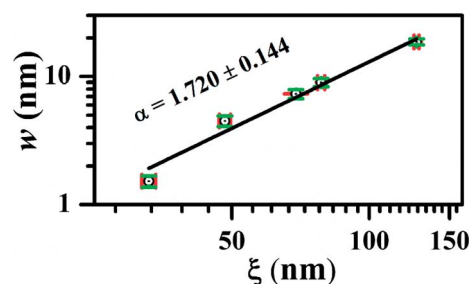

Fig. 5 log–log plot of w versus ξ showing linear behavior.

behavior can be classified by Ramasco *et al.*[36] into four probable categories, namely, (i) $\alpha_s < 1$, $\alpha_{loc} = \alpha_s = \alpha$, corresponds to Family–Vicsek standard scaling; (ii) for $\alpha_s > 1$, $1 = \alpha_{loc} \neq \alpha_s = \alpha$, super-rough scaling; (iii) $\alpha_s < 1$, $\alpha_{loc} = \alpha_s \neq \alpha$, called intrinsic anomalous scaling; and (iv) $\alpha_s > 1$, $\alpha_{loc} \neq \alpha_s \neq \alpha \neq 1$ suggest a new class of scaling.

Fig. 6(a) shows log–log plot of PSD(k) *versus* k of the surfaces from the representative AFM images of MoS$_2$ films deposited on glass substrates for the duration of 20 s, 1, 2, 5, 10 and 15 min. The PSD function does not show any characteristics peak at k_m inferring that the film grew as self-affine surface and not mounded.[37] In the PSD spectra two distinct regions, $k < t^{-1/z}$ and $k > t^{-1/z}$ represented by eqn (3) are clearly visible. At lower k values PSD(k) is almost saturated for all the films while at higher k regimes PSD(k) value linearly decreases with k as PSD(k) $\sim k^{-(2\alpha_s+d)}$ where $d = 2$ in our case. PSD value increases with deposition time and the transition point between linearly decreasing and saturated regions which corresponds to $\sim 1/\xi$ are shifted towards lower k regimes corresponds to an increase in island size ($\sim\xi$) of the MoS$_2$ films with time.

Fig. 6(b) shows the values of α_s estimated from the slope of each PSD(k) plots (except that of the film deposited for 20 s) from $k > t^{-1/z}$ regime. The average value α_s for the MoS$_2$ films was observed to be $\sim 0.85 \pm 0.03$. The relevant exponents α, α_s and α_{loc} required for classifying the category of scaling are obtained from above analysis which shows that α_{loc} (0.89 ± 0.01) $\sim \alpha_s$ (0.85 ± 0.03) $\neq \alpha$ (1.72 ± 0.14) and $\alpha_s < 1$. This indicates an intrinsic anomalous scaling behavior for surface growth of the MoS$_2$ thin films.[36,43] Fig. 6(c) exhibits 2D fast Fourier transform (FFT) of AFM images corresponding to MoS$_2$ films deposited for 1 min and 10 min. It shows a diffuse structure and absence of any bright ring like structure in k-space which support the self-affine like growth morphology excluding any type of mound formation in the surface of the films during growth.[45]

In order to further verify the anomalous scaling behavior of growth of the MoS$_2$ films, we investigated the collapse of the HHCF and PSD dependent functions for different growth times. Under anomalous scaling, HHCF is given as,[46]

$$H(r,t) = r^{2\alpha} g_A\left(r\big/t^{\frac{1}{z}}\right) \tag{4}$$

where the anomalous scaling function, $g_A\left(r\big/t^{\frac{1}{z}}\right)$, behaves as,

$$g_A\left(r\big/t^{\frac{1}{z}}\right) \sim \begin{cases} \left(r\big/t^{\frac{1}{z}}\right)^{-2(\alpha-\alpha_{loc})}, & r\big/t^{\frac{1}{z}} \ll 1 \\ \left(r\big/t^{\frac{1}{z}}\right)^{-2\alpha}, & r\big/t^{\frac{1}{z}} \gg 1 \end{cases}$$

Hence the function $H(r,t)/r^{2\alpha}$ when plotted as a function of $\left(r\big/t^{\frac{1}{z}}\right)$ in log–log scale for different deposition times should collapse into single curve and from their slopes both α and α_{loc} can be estimated.[39] Similarly, PSD function can also be expressed under anomalous scaling as,[39,46]

$$PSD(k,t) = k^{-(2\alpha+d)} \psi_A\left(kt^{\frac{1}{z}}\right) \tag{5}$$

where the spectral scaling function, $\psi_A\left(kt^{\frac{1}{z}}\right)$, behaves as,

$$\psi_A\left(kt^{\frac{1}{z}}\right) \sim \begin{cases} \left(kt^{\frac{1}{z}}\right)^{2\alpha+d}, & kt^{\frac{1}{z}} \ll 1 \\ \left(kt^{\frac{1}{z}}\right)^{2(\alpha-\alpha_s)}, & kt^{\frac{1}{z}} \gg 1 \end{cases}$$

Hence the function PSD(k,t)$k^{(2\alpha+d)}$ when plotted as a function of $\left(kt^{\frac{1}{z}}\right)$ in log–log scale for different deposition times should collapse into one curve and from their slopes both α and α_s can be estimated. For our case, $d = 2$, hence PSD(k,t) = $k^{(2\alpha+2)} \psi_A\left(kt^{\frac{1}{z}}\right)$.[39] Fig. 7(a) and (b) exhibit the plot of log $H(r,t)/r^{2\alpha}$ *versus* $\log\left(r\big/t^{\frac{1}{z}}\right)$ and plot of log PSD(k,t)$k^{(2\alpha+2)}$ *versus* $\log\left(kt^{\frac{1}{z}}\right)$, respectively for the MoS$_2$ films deposited for various time period (1–15 min). In Fig. 7(a), all the curves corresponding to different time period of growth collapsed to
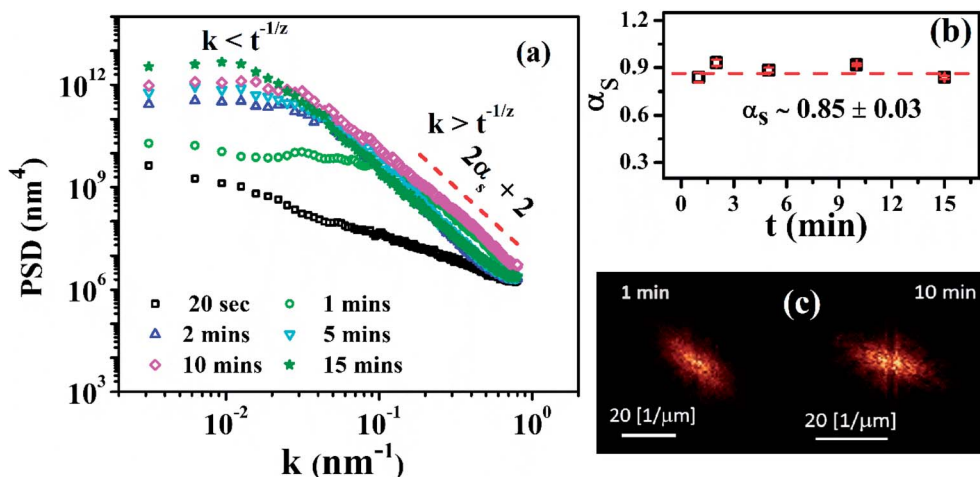

Fig. 6 log–log plot of (a) PSD(k) as a function of k for MoS$_2$ thin films deposited on the glass substrate with different deposition times. (b) Plot of α_s of the MoS$_2$ films as a function of deposition time. (c) 2D FFT pattern of the AFM images of MoS$_2$ films deposited for 1 and 10 min.

a single curve confirming the existence of anomalous scaling with slope values of 2 $(\alpha - \alpha_{\text{loc}}) \sim 1.66 \pm 0.01$ and $2\alpha \sim 3.42 \pm 0.02$, for $r/t^{1/z} \ll 1$ and $r/t^{1/z} \gg 1$, respectively. From these slope the values of α and α_{loc} are estimated to be 1.71 ± 0.01 and 0.88 ± 0.01, respectively, which are similar to their respective values obtained directly from HHFC analysis discussed above. Similarly, in Fig. 7(b), the collapse of all the PSD related curves, corresponding to different time period of growth, to a single curve confirming the existence of anomalous scaling with slope values of $(2\alpha + 2) \sim 5.40 \pm 0.17$ for $kt^{1/z} \ll 1$ and $2(\alpha - \alpha_{\text{s}}) \sim 1.69 \pm 0.02$ for $kt^{1/z} \gg 1$, respectively.[39] The values of α and α_{s} were extracted from the average values of slopes and are found to be 1.70 ± 0.08 and 0.85 ± 0.01, respectively. The values of α and α_{s} obtained from the collapse of the PSD functions are also in agreement with the values obtained above. The inequality in $\alpha > 1 > \alpha_{\text{loc}} \sim \alpha_{\text{s}}$ reconfirms the presence of intrinsic anomalous scaling in the present case.

Different local models like Mullins diffusion model,[47] Edwards–Wilkinson model[48] and KPZ model[49] provide $\beta = 0.25$, 0 and 0.24, $\alpha = 1$, 0 and 0.38 while $z = 4$, 2 and 1.58, respectively for 2 + 1 dimensions which does not match with the values of β, α and z observed in present case. Thus, none of the local models depicting different universality class can exactly explain the type of growth observed here. Although the exact mechanism has not been well understood, some studies in recent years have proposed that the anomalous kinetic roughening of the surfaces with a high growth exponent arises as consequences of nonlocal effects.[50] Yao and Guo[51] modified the non-local KBR model[52] in sputtering growth where shadowing instability leads to the development of a mounded surface resulting $w \sim t^{1.0 \pm 0.04}$ and $\xi \sim t^{0.33 \pm 0.02}$. Moreover, Drotar et al.[53] modeled the growth of a surface under shadowing (roughening effect) and higher zeroth-order sticking coefficient corresponds to minimal reemission ($s_0 = 1$ and $s_n = 0$ for $n > 0$), using a stochastic continuum growth equation,

$$\frac{\partial h}{\partial t} = v\nabla^2 h(r,t) - k\nabla^4 h(r,t) + s_0 F_0(r,t)\sqrt{1 + |\nabla h|^2} + \eta(r,t), \quad (6)$$

with

$$F_0 = \int_0^{2\pi} \int_0^{\theta_{\max}} R(\theta, \Phi)[\sin\theta(\hat{i}\cos\Phi + \hat{j}\sin\Phi) + \hat{j}\cos\theta]$$

$$\hat{n}(r)(\sin\theta)d\theta d\Phi$$

, where θ is the local polar angle, Φ is the local azimuthal angle and $R(\theta,\Phi)$ is the distribution of the incoming flux. They simulated the film surface growth using eqn (6) by Monte Carlo method in 2 + 1 dimensions giving $\beta = 1$ and $1/z = 0.93 \pm 0.01$. The β value predicted by the model formulated by Yao et al.[51] and Drotar et al.[53] is close to the present work ($\beta = 0.88 \pm 0.07$) while the $1/z$ value ($1/z = 0.51 \pm 0.08$) is in between their reported values. As PLD process is directional, (flux distribution $\sim \cos^p \theta$) substrate receives incoming species at wide distribution of angle varying from 0° to nearly $\theta_{1/2}$ ($=\cos^{-1}(1/2)^p$).[54] $\theta_{1/2}$ is the angle between target surface normal and flux direction where flux density becomes half of maximum in vacuum and p (varies from 8–20) is the parameter decided by laser spot size, laser fluence and degree of ionization of plasma.[54] Hence, growth process occurs overwhelmingly under shadowing mechanism due to angle dependent variable particle flux density. Hence these deposition conditions promoting large shadowing and high sticking coefficient of substrate (due to high substrate temperature of 600 °C) which are suitable for surface growth under the non-local models discussed above.[53]

3.3. Optical characterization of MoS$_2$ films using spectroscopic ellipsometric studies

In any ellipsometric experiment, the changes in the state of the polarization of an incident beam, upon reflection from the sample surface, is measured. The changes are expressed in terms of two parameters, ψ and Δ, given by the following equation,[55]

$$\rho = \frac{r_{\text{p}}}{r_{\text{s}}} = \left|\frac{r_{\text{p}}}{r_{\text{s}}}\right| e^{i(\Delta_{\text{p}} - \Delta_{\text{s}})} = \tan\psi\, e^{i\Delta} \quad (7)$$

where r_{p} and r_{s} are the Fresnel reflection coefficients for a plane wave polarized parallel (p) and perpendicular (s) to the plane of incidence, respectively while Ψ and Δ are the ellipsometric angles. Ψ is the angle whose tangent gives the ratio of the magnitude of the reflection coefficient of electric field components along the p and s polarizations and Δ gives the difference
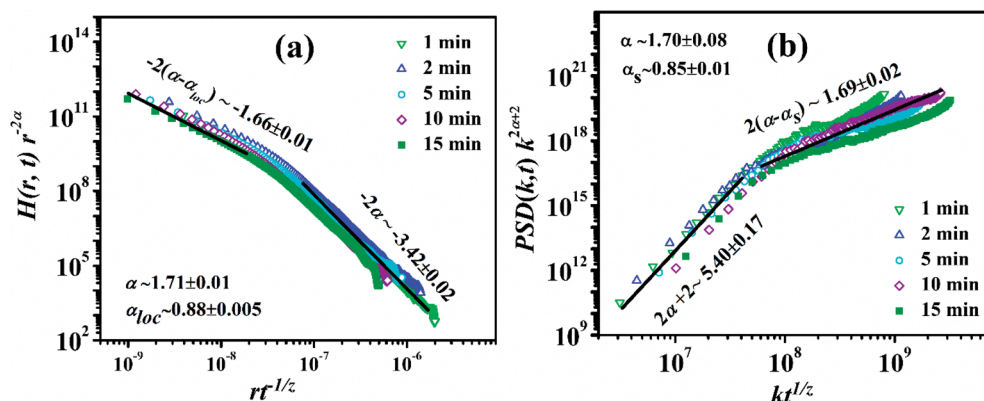

Fig. 7 Plots of (a) log $H(r,t)/r^{2\alpha}$ versus log$(r/t^{\frac{1}{z}})$ and (b) log PSD$(k,t)k^{(2\alpha+2)}$ versus log$(kt^{\frac{1}{z}})$ showing data collapse of the anomalous scaling functions of the MoS$_2$ films deposited for different time periods.

between the phase shifts of electric field components of p and s polarizations, Δ_p and Δ_s, experienced upon reflection. The ellipsometric parameters $\cos(\Delta)$ and $\tan(\psi)$ are directly recorded as a function of wavelength at different angles of incidence. In the particular case of an abrupt interface between two semi-infinite media the ellipsometric data are related to the pseudo complex dielectric function ε by the following relation[55]

$$\varepsilon = \varepsilon_1 + i\varepsilon_2 = \sin^2\Phi\{1 + [(1-\rho)/(1+\rho)]^2\tan^2\Phi\} \qquad (8)$$

where Φ is the angle of incidence. Using eqn (7) and (8), the real (ε_1) and imaginary (ε_2) part of pseudo dielectric function can be expressed as a function of Δ and ψ. Hence n and k spectra can also be estimated from ellipsometric parameters (Δ and ψ). These spectra are fitted to appropriate optical models and suitable layered structure to obtain the parameters of the dispersion model, thickness, n and k. According to the sample structures in this work, the SE spectra were analyzed by considering a four-layered model from top to bottom as ambient/roughness/MoS$_2$/Corning glass substrate. The roughness layer was modeled using Bruggeman effective medium approximation (BEMA) for a mixture composed of 50% MoS$_2$ and 50% voids within top roughness layer. Here for MoS$_2$ part, a dispersion relation using two Lorentz oscillators is used while for void part its n–k file from SEA database was used. For the film layer which is sandwiched between the top layer and substrate, a dispersion relation using four Lorentz oscillators was used while for Corning glass and ambient n–k file from database of SEA software was employed to fit the experimental ψ and Δ spectra for all MoS$_2$ films. The real (ε_1) and imaginary (ε_2) part of dielectric permittivity considering Lorentz model are defined as,

$$\varepsilon_1(E) = \frac{fE_0^2(E_0^2 - E^2)}{(E_0^2 - E^2)^2 + \Gamma^2 E^2}$$

and $\qquad\qquad\qquad\qquad\qquad\qquad\qquad (9)$

$$\varepsilon_2(E) = \frac{fE_0^2 \Gamma E}{(E_0^2 - E^2)^2 + \Gamma^2 E^2}$$

where E is the photon energy and f, E_0, Γ are the oscillator amplitude/strength, oscillator position and damping coefficient of Lorentz oscillator in eV.

Fig. 8(a) and (b) shows ψ and Δ spectra of the MoS$_2$ films fitted with the four-layered model described in the optical energy range of 1.5–3.5 eV. All the curves shows good fitting with average root means square error (RMSE) value $\sim$ 0.7. The ψ value of MoS$_2$ films deposited for 15, 10 and 5 min increases in higher optical energy region while that of 1 and 2 min shows the opposite trend. The overall Δ increases with the increasing deposition time.

The Bruggeman effective medium approximation (BEMA) model used for top layer of MoS$_2$ films provides two parameters called the layer thickness (d_s) and the fraction of the species (f_v – 50%, fixed in our analysis). The value of d_s is generally assumed to reflect the RMS roughness of the real surface. So far, there is no established straightforward relation between the RMS roughness, w and d_s, obtained from AFM images and

ellipsometric analysis of the thin films, respectively. A linear correlation between w and d_s was estimated by Fujiwara et al. for a-Si:H films thought they also reported different w/d_s ratios for different growth condition even for the same material.[56,57] In case of self-affine surfaces, the BEMA roughness (d_s) is given as the product of average surface slope ($\delta \sim w/\xi^\alpha$) and the AFM surface roughness (ω), $d_s \sim \omega\delta$.[58] The average surface slope is expected to remain constant for films following dynamic scaling. On the other hand for anomalous scaling δ is not constant but varies with time as $\delta \sim t^k$, where k is a constant for a set of films deposited for different duration.[59] The values of d_s estimated from BEMA for MoS$_2$ films fabricated at different deposition duration were not similar to that of w (Fig. 3(b)) for each film.

Fig. 9 exhibits the variation of d_s as a function of w which shows that d_s does not vary linearly with w and their slope ($\sim\delta$) also varies with time. The inset shows the log–log plot of δ vs. t where their slope $k = 0.36 \pm 0.04$. The δ estimated from growth exponents ($\delta \sim w/\xi^\alpha$) extracted from AFM analysis also scales with t as $\delta \sim t^{0.43\pm0.01}$ which is close to that of estimated from slope of d_s vs. w curve. The behavior of average local slope, $\delta \sim t^{0.36\pm0.04}$, reconfirms presence of anomalous scaling of growth exponents during the PLD of the MoS$_2$ films. Now, let us consider the SE analysis of main MoS$_2$ layer, sandwiched between top roughness layer and the Corning glass substrate, for which a dispersion relation using four Lorentz oscillators was used. The thickness of the main MoS$_2$ layer, estimated from SE analysis, were found to be $\sim$2.1, 5.5, 15.7, 37 and 77 nm for films deposited for 1, 2, 5, 10 and 15 min, respectively, which are similar to that measured from the profilometer.

Fig. 10(a) and (b) shows the n and k spectra of the main MoS$_2$ layer. Both refractive index (n) and extinction coefficient (k) spectra shows an overall increase with increasing deposition duration. The n and k spectra are nearly similar to that reported by Yim et al. for MoS$_2$ films deposited on SiO$_2$/Si substrate by vapor phase sulfurization process.[60] The k spectra show absorption peak in the range of 2.8–3.3 eV corresponding to C/D excitonic transitions. ESI Fig. S3† exhibits variation of (a) amplitudes (f_1, f_2, f_3 and f_4) and (b) broadening parameters (Γ_1, Γ_2, Γ_3 and Γ_4) of four Lorentz oscillators, used to describe the dispersion law for the MoS$_2$ film layer, as a function of deposition duration. For all the four oscillators their oscillator amplitude/strength were observed to increase with increasing deposition duration and thickness which is an indicative of formation of denser films at longer deposition times.[55] Moreover, from AFM images (Fig. 2) it was observed that at early stage of film growth MoS$_2$ clusters are sparsely distributed throughout the film but at longer deposition duration, densely packed larger clusters were formed. This morphology variation as a function of deposition duration is due to addition of new nucleation centers as well as continuous growth of already formed nuclei formed at early stages of film growth. The increase in coverage of film and cluster size ($\sim\xi$) with increasing deposition duration results in decrease in void density and consequent increase in material density of film. From ESI Fig. S3(b),† a gradual decrease in broadening parameter was also observed with t. In our result, the correlation length (ξ) and
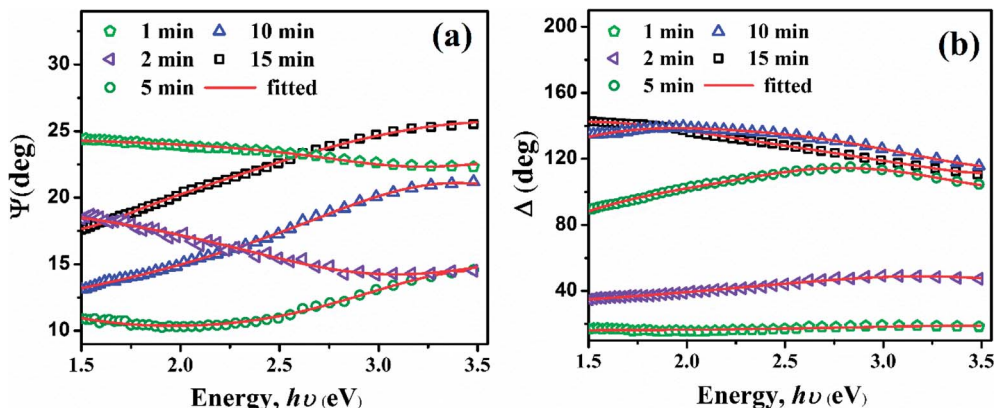
Fig. 8 Plots of experimental and simulated SE parameters – (a) ψ and (b) Δ spectra of the MoS$_2$ films fabricated for 1 to 15 min.
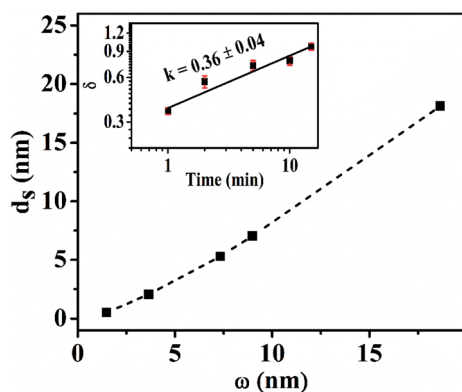

Fig. 9 Plot of d_s vs. w with an inset showing of δ vs. t in log−log scale.

crystalline grain size (shown by XRD analysis, ESI Fig. S1†) of the MoS$_2$ films also grows with deposition time. Hence, the decline in Γ_1, Γ_2, Γ_3 and Γ_4 with t can be viewed as a result of increasing ξ (Fig. 3(c)). The result is quite similar to the reported decrease in broadening parameter with the grain size of poly-crystalline and microcrystalline silicon thin films.[61] The broadening of Lorentz oscillator is a consequence of surface scattering and lattice defect which represents the structural

disorder in a sample. Thus, the reduction in Lorentz broad-ening parameter with growth time in the film indicates an increase in their structural order and hence enhancement in crystallinity of films was observed with increasing ξ. This enhanced structural order and crystallinity results in increased film compactness and density for thicker films. Now, consid-ering similar layered model as above (depicted in ESI Fig. S4(a)†) and considering BEMA for middle layer (sand-wiched between the top roughness layer and substrate) composed of voids and a MoS$_2$ dispersion matrix, the void percentages within the films were estimated from SE data (details provided in ESI†).[62] The void fraction present in the MoS$_2$ films deposited for 1, 2, 5, 10 and 15 min are found to be 15.6, 14.1, 13.6, 8.8 and 6.0%, respectively, exhibiting decrease in void% with thickening of the film as depicted in ESI Fig. S4(b).†[63] The increase in n with increasing deposition duration is due to increase in film density which is well sup-ported by above observations. The increase in k with increasing deposition duration can also be explained as a result of an increase in the film density as well as their increasing RMS roughness. The increased surface roughness might have facili-tated increased absorption due to increased surface area and enhanced light matter interaction due to local field effect.
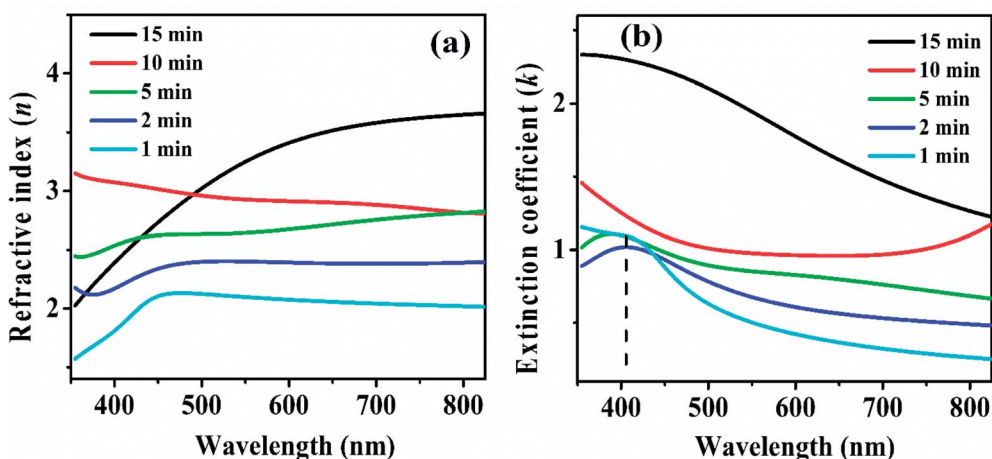

Fig. 10 Plots of (a) n and (b) k spectra of MoS$_2$ films deposited for different time durations.

Hence both w and ξ seem to play a vital role in controlling the optical parameters of MoS_2 films during their growth.

4. Conclusions

In the present work, the kinetic roughening of MoS_2 thin films grown by the PLD technique has been studied based on generic scaling *ansatz* using surface morphology information from AFM images of the films. The characteristic exponents $\alpha_{loc} = 0.89 \pm 0.05$, $\alpha = 1.72 \pm 0.11$, $\alpha_s = 0.85 \pm 0.03$, $1/z = 0.49 \pm 0.11$ and $\beta = 0.85 \pm 0.09$ were determined using the HHCF and PSD functions. The local slope increases with growth time as, $m \sim t^{\beta^*}$. The value $\beta^* \sim 0.41 \neq 0$ confirms that anomalous scaling has occurred. The anomalous scaling functions related to both HHCF and PSD for films deposited for different time periods collapsed to respective single curve confirming the presence of definite anomalous scaling during MoS_2 film growth under PLD. These analyses revealed presence of intrinsic anomalous scaling of roughness with rapid roughening of the surfaces as $\alpha_s < 1 < \alpha$, $\alpha_{loc} \sim \alpha_s \neq \alpha$. The growth exponents ($\alpha_{loc}$, β and $1/z$) estimated in present case cannot be exactly related to any known universality classes based on both local and non-local growth models, suggesting that a different universality class needed to be defined. The models considering nonlocal effects like shadowing plays an important role in the evolution of growth front of these PLD thin films. The observed anomalous scaling behavior is also supported by the relation $\delta \sim t^{0.36 \pm 0.04}$ extracted from SE studies. Moreover the SE studies also suggest that the optical functions (n and k) increases during film growth depending on the evolution of w and ξ with t as they control their surface area and the film density.

Conflicts of interest

There are no conflicts of interest to declare.

Acknowledgements

References

1 X. Song, J. Hu and H. Zeng, *J. Mater. Chem. C*, 2013, **1**, 2952–2969.

2 Q. H. Wang, K. Kalantar-Zadeh, A. Kis, J. N. Coleman and M. S. Strano, *Nat. Nanotechnol.*, 2012, **7**, 699–712.

3 M. Xu, T. Liang, M. Shi and H. Chen, *Chem. Rev.*, 2013, **113**, 3766–3798.

4 K. F. Mak, C. Lee, J. Hone, J. Shan and T. F. Heinz, *Phys. Rev. Lett.*, 2010, **105**, 136805.

5 A. Splendiani, L. Sun, Y. Zhang, T. Li, J. Kim, C.-Y. Chim, G. Galli and F. Wang, *Nano Lett.*, 2010, **10**, 1271–1275.

6 I. Song, C. Park and H. C. Choi, *RSC Adv.*, 2015, **5**, 7495–7514.

7 Y. Yoon, K. Ganapathi and S. Salahuddin, *Nano Lett.*, 2011, **11**, 3768–3773.

8 L. Liu, S. B. Kumar, Y. Ouyang and J. Guo, *IEEE Trans. Electron Devices*, 2011, **58**, 3042–3047.

9 B. Radisavljevic, A. Radenovic, J. Brivio, V. Giacometti and A. Kis, *Nat. Nanotechnol.*, 2011, **6**, 147–150.

10 Y. Zhang, J. Ye, Y. Matsuhashi and Y. Iwasa, *Nano Lett.*, 2012, **12**, 1136–1140.

11 H. Qiu, L. Pan, Z. Yao, J. Li and Y. Shi, *Appl. Phys. Lett.*, 2012, **100**, 123104.

12 Z. Yin, H. Li, H. Li, L. Jiang, Y. Shi, Y. Sun, G. Lu, Q. Zhang, X. Chen and H. Zhang, *ACS Nano*, 2011, **6**, 74–80.

13 H. Wang, L. Yu, Y.-H. Lee, Y. Shi, A. Hsu, M. L. Chin, L.-J. Li, M. Dubey, J. Kong and T. Palacios, *Nano Lett.*, 2012, **12**, 4674–4680.

14 J. Deng, W. Yuan, P. Ren, Y. Wang, D. Deng, Z. Zhang and X. Bao, *RSC Adv.*, 2014, **4**, 34733–34738.

15 M. He, F. Kong, G. Yin, Z. Lv, X. Sun, H. Shi and B. Gao, *RSC Adv.*, 2018, **8**, 14369–14376.

16 X. Chen, J. Ding, J. Jiang, G. Zhuang, Z. Zhang and P. Yang, *RSC Adv.*, 2018, **8**, 29488–29494.

17 T. A. Loh and D. H. Chua, *ACS Appl. Mater. Interfaces*, 2014, **6**, 15966–15971.

18 D. J. Late, P. A. Shaikh, R. Khare, R. V. Kashid, M. Chaudhary, M. A. More and S. B. Ogale, *ACS Appl. Mater. Interfaces*, 2014, **6**, 15881–15888.

19 G. Nabiyouni and B. J. Farahani, *Appl. Surf. Sci.*, 2009, **256**, 674–682.

20 M. Al-Kuhaili, *J. Phys. D: Appl. Phys.*, 2007, **40**, 2847.

21 J. Jeffries, J.-K. Zuo and M. Craig, *Phys. Rev. Lett.*, 1996, **76**, 4931.

22 G. Palasantzas and J. Krim, *Phys. Rev. Lett.*, 1994, **73**, 3564.

23 M. Pelliccione, T. Karabacak, C. Gaire, G.-C. Wang and T.-M. Lu, *Phys. Rev. B: Condens. Matter Mater. Phys.*, 2006, **74**, 125420.

24 G. Lengel, R. Phaneuf, E. Williams, S. D. Sarma, W. Beard and F. Johnson, *Phys. Rev. B: Condens. Matter Mater. Phys.*, 1999, **60**, R8469.

25 N. M. Das, D. Roy, N. Clarke, V. Ganesan and P. S. Gupta, *RSC Adv.*, 2014, **4**, 32490–32503.

26 P. P. Chatraphorn, Z. Toroczkai and S. D. Sarma, *Phys. Rev. B: Condens. Matter Mater. Phys.*, 2001, **64**, 205407.

27 A.-L. Barabási and H. E. Stanley, *Fractal concepts in surface growth*, Cambridge University Press, 1995.

28 Y. P. Zhao, J. Fortin, G. Bonvallet, G. C. Wang and T. M. Lu, *Phys. Rev. Lett.*, 2000, **85**, 3229.

29 A. R. Forouhi and I. Bloomer, *Phys. Rev. B: Condens. Matter Mater. Phys.*, 1986, **34**, 7018–7026.

30 S. Adachi, *Phys. Rev. B: Condens. Matter Mater. Phys.*, 1988, **38**, 12345–12352.

31 G. E. Jellison and F. A. Modine, *Appl. Phys. Lett.*, 1996, **69**, 371–373.

32 J. Tauc, R. Grigorovici and A. Vancu, *Phys. Status Solidi B*, 1966, **15**, 627–637.

33 C. Lee, H. Yan, L. E. Brus, T. F. Heinz, J. Hone and S. Ryu, *ACS Nano*, 2010, **4**, 2695–2700.

34 M. Ye, D. Winslow, D. Zhang, R. Pandey and Y. Yap, 2015.

35 T. A. Loh and D. H. Chua, *Chem. Phys. Lett.*, 2014, **610**, 284–287.

36 J. J. Ramasco, J. M. López and M. A. Rodríguez, *Phys. Rev. Lett.*, 2000, **84**, 2199–2202.

37 M. Pelliccione and T. M. Lu, *Evolution of Thin Film Morphology: Modeling and Simulations*, Springer-Verlag New York, New York, 1st edn, 2008.

38 K. L. Chopra, *Thin Film Phenomena*, McGraw-Hill Book Company, New York, 1969.

39 M. Nasehnejad, G. Nabiyouni and M. G. Shahraki, *J. Phys. D: Appl. Phys.*, 2017, **50**, 375301.

40 I. Gupta and B. C. Mohanty, *Sci. Rep.*, 2016, **6**, 33136.

41 M. Saitou, *Phys. Rev. B: Condens. Matter Mater. Phys.*, 2002, **66**, 073416.

42 S. Das Sarma, C. J. Lanczycki, R. Kotlyar and S. V. Ghaisas, *Phys. Rev. E: Stat., Nonlinear, Soft Matter Phys.*, 1996, **53**, 359–388.

43 J. M. López, M. A. Rodríguez and R. Cuerno, *Phys. Rev. E: Stat., Nonlinear, Soft Matter Phys.*, 1997, **56**, 3993–3998.

44 J. M. López, *Phys. Rev. Lett.*, 1999, **83**, 4594–4597.

45 S. M. Obaidulla and P. Giri, *Appl. Phys. Lett.*, 2015, **107**, 221910.

46 M. F. Torres and R. C. Buceta, *Eur. Phys. J. B*, 2013, **86**, 20.

47 W. W. Mullins, *J. Appl. Phys.*, 1957, **28**, 333–339.

48 S. F. Edwards and D. R. Wilkinson, *Proc. R. Soc. London, Ser. A*, 1982, **381**, 17–31.

49 M. Kardar, G. Parisi and Y.-C. Zhang, *Phys. Rev. Lett.*, 1986, **56**, 889.

50 J. M. López, M. Castro and R. Gallego, *Phys. Rev. Lett.*, 2005, **94**, 166103.

51 J. H. Yao and H. Guo, *Phys. Rev. E: Stat. Phys., Plasmas, Fluids, Relat. Interdiscip. Top.*, 1993, **47**, 1007.

52 R. Karunasiri, R. Bruinsma and J. Rudnick, *Phys. Rev. Lett.*, 1989, **62**, 788.

53 J. T. Drotar, Y.-P. Zhao, T.-M. Lu and G.-C. Wang, *Phys. Rev. B: Condens. Matter Mater. Phys.*, 2000, **62**, 2118.

54 I. Weaver and C. Lewis, *J. Appl. Phys.*, 1996, **79**, 7216–7222.

55 H. Fujiwara, *Spectroscopic ellipsometry: principles and applications*, John Wiley & Sons, 2007.

56 H. Fujiwara, M. Kondo and A. Matsuda, *Phys. Rev. B: Condens. Matter Mater. Phys.*, 2001, **63**, 115306.

57 H. Fujiwara, J. Koh, P. Rovira and R. Collins, *Phys. Rev. B: Condens. Matter Mater. Phys.*, 2000, **61**, 10832.

58 M. Losurdo and K. Hingerl, *Ellipsometry at the Nanoscale*, Springer, 2013.

59 G. Palasantzas, *Phys. Rev. E: Stat. Phys., Plasmas, Fluids, Relat. Interdiscip. Top.*, 1997, **56**, 1254.

60 C. Yim, M. O'Brien, N. McEvoy, S. Winters, I. Mirza, J. G. Lunney and G. S. Duesberg, *Appl. Phys. Lett.*, 2014, **104**, 103114.

61 S. Logothetidis, *J. Appl. Phys.*, 1989, **65**, 2416–2426.

62 P. McMarr, J. Blanco, K. Vedam, R. Messier and L. Pilione, *Appl. Phys. Lett.*, 1986, **49**, 328–330.

63 S. T. Sundari, S. Dash and A. Tyagi, *presented in part at International Conference on Nanoscience, Engineering and Technology (ICONSET 2011)*, Chennai, November, 2011.